Available online at www.sciencedirect.com
ScienceDirect
Ceramics International 37 (2011) 2519–2526
CERAMICS INTERNATIONAL
www.elsevier.com/locate/ceramint

Effect of Tb substitution on structural, magnetic and electrical properties of magnesium ferrites

M. Azhar Khan [a,*], M.U. Islam [a], M. Ishaque [a], I.Z. Rahman [b]

[a] Department of Physics, Bahauddin Zakariya University, Multan 60800, Pakistan
[b] Department of Physics, Materials and Surface Science Institute (MSSI), University of Limerick, National Technological Park, Limerick, Ireland

Received 30 January 2011; received in revised form 21 March 2011; accepted 31 March 2011
Available online 8 April 2011

Abstract

A series of $Mg_{1-x}Tb_xFe_2O_4$, ferrite samples ($0.0 \leq x \leq 0.2$) were synthesized by the ceramic method and were characterized by using X-ray diffraction, Fourier transform infrared spectroscopy (FTIR) and vibrating sample magnetometery. The XRD patterns showed the single phase ferrites up to $x \leq 0.04$ without other secondary phase. The lattice constant increases slightly as a function of terbium content up to $x = 0.04$ and decreases for $x > 0.04$. The increase is attributed to the difference in the ionic radii of the cations involved and decrease led to the formation of secondary phase ($TbFeO_3$). The bulk density was found to increase from 3.5 to 4.6 (g/cm^3) with the increase of terbium concentration. FTIR spectra exhibited two significant absorption bands in the wave number range of 370–1500 cm^{-1} which confirm the spinel structure and completion of chemical reaction. The magnetic properties revealed a decrease in the saturation magnetization as a function of Tb content. An unexpected increase in magnetization at the Tb content of 0.02 could be due to the migration of Mg ions towards tetrahedral sites, consistent with the results of FTIR. Coercivity variations are attributed to the magneto-crystalline anisotropy. The resistivity increased with the substitution of terbium relative to the sample undoped with terbium while the drift mobility was found to decrease.

Keywords: A. Powders: solid state reaction; C. Magnetic properties; C. Electrical properties; E. Soft magnets

1. Introduction

The properties of ferrites strongly depend on the chemical composition, cation distribution, method of preparation in general and structure in particular. The soft magnetic behaviour in ferrites is caused by the exchange interaction among the cations on the polyhedral sites. The rare earth cations, having their 4f orbital totally screened by 5s and 5p orbital and these play a key role in deciding the electrical and magnetic properties of ferrites [1,2]. The rare earth substituted ferrites find potential applications in modern telecommunications and electronic devices [3]. Mg–Zn ferrites have been reported to be industrially useful in the fabrication of cores of intermediate frequency transformer and antenna [4]. Magnesium ferrites are pertinent magnetic material and are used in variety of applications; transformers, magnetic core coils and ferrofluids. This ferrite is also used in achieving thermal coagulation therapy, in which tumors are locally heated by the application of an alternating magnetic field [5,6]. The rare earth substituted Mg-ferrites having high resistivity are suitable candidates for high frequency applications. These ferrites are used in television yokes and fly back transformers because of their high resistivity which eliminates the need for taped insulation between yoke and winding [7].

The main aim of the present communication is to study the influence of replacing Mg ions by Tb ions on the structural, magnetic and electrical properties of $Mg_{1-x}Tb_xFe_2O_4$ ferrite in details. Since Tb-substituted Mg-ferrite have not been investigated frequently, in the present study the mentioned properties of $Mg_{1-x}Tb_xFe_2O_4$ ferrites have been reported in order to cater for the above applications.

2. Experimental details

Polycrystalline terbium substituted magnesium ferrites with chemical formula $Mg_{1-x}Tb_xFe_2O_4$ ($x = 0$, 0.02, 0.04, 0.06, 0.08, 0.1, 0.12, 0.14, 0.16, 0.18, 0.20) were prepared by

* Corresponding author. Tel.: +92 61 9210091; fax: +92 619210068.
E-mail address: azhar_manais@hotmail.com (M.A. Khan).

0272-8842/$36.00
doi:10.1016/j.ceramint.2011.03.063

standard ceramic technique. The starting materials were analytical reagent grade oxide powders of MgO, Tb_4O_7 and Fe_2O_3 (99.99% pure) supplied by Aldrich. The initial ingredients were intimately mixed in stoichiometric proportions to yield desired compositions and ground for 3 h using an agate mortar and pestle to a fine powder. The powder mixtures were cold pressed into pellets using a hydraulic pressing machine (Paul–Otto–Weber) under the load of 30 kN. The green samples in the form of pellets were initially sintered at 1000 °C for 48 h and finally sintered for 6 h at 1230 °C for obtaining a homogenous product followed by air quenching.

X-ray diffraction patterns were recorded to identify the phases formed and to confirm the completion of chemical reaction. Philips X-ray diffractometer (XPert MPD) operated at 40 kV and 35 mA with Cu K_α radiation ($\lambda = 1.540562$ Å) at room temperature was used. The lattice constant '*a*' for each sample was calculated using Nelson–Riley extrapolation method. The values of the lattice parameters were obtained for each reflected plane plotted against the Nelson–Riley function [8];

$$F(\theta) = \frac{1}{2}\left[\frac{\cos^2\theta}{\sin\theta} + \frac{\cos^2\theta}{\theta}\right] \quad (1)$$

where θ is the Bragg's reflection and straight lines were obtained. The accurate value of lattice parameter was obtained from the extrapolation of the line to $F(\theta) = 0$ or $\theta = 90^\circ$. The X-ray densities were calculated using the relation [9];

$$D_x = \frac{8M}{Na^3} \quad (2)$$

where M is the molecular weight of the sample, a the lattice constant and N the Avogadro's number. Physical properties were measured after cleaning both sides of the pellets by grinding on SiC paper of micron size in order to remove 0.3 mm thick oxide layer. The bulk density D_b (g/cm^3) of each composition was measured using toluene by Archimedes principle. The percentage porosity of the samples was calculated using the following relation;

$$P = \left(1 - \frac{D_b}{D_x}\right) \times 100 \quad (3)$$

where D_b and D_x are the bulk and X-ray density, respectively.

Perkin Elmer FTIR Spectrometer (Spectrum 2000) was used to observe the IR spectra at room temperature over the wave number range 370–1500 cm^{-1}. The samples were prepared in the form of pellets in KBr medium.

The M–H loops were plotted at room temperature. The computer controlled vibrating sample magnetometer (VSM); LakeShore model 7300 was used in which the sample was vibrated vertically between pickup coils in a constant magnetic field. The vibrating sample magnetometer was calibrated with a Ni-standard 3.475 emu 5000G. The dc resistivity of all the samples at different temperatures was measured by two probe method in the temperature range of 303–473 K.

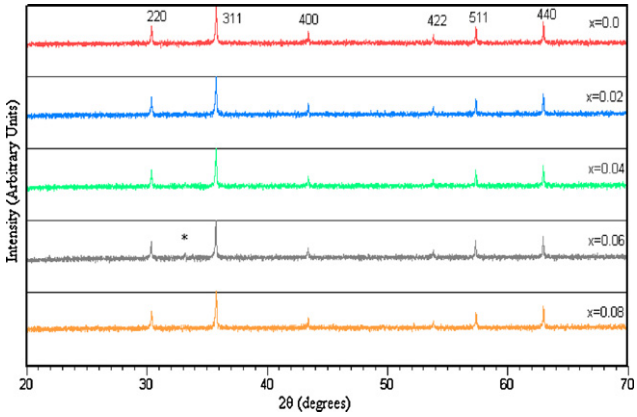

Fig. 1. X-ray diffraction patterns for $Mg_{1-x}Tb_xFe_2O_4$ ferrites ($x = 0.0$, 0.02, 0.04, 0.06, 0.08).

3. Results and discussion

3.1. Structural properties

X-ray diffractograms of $Mg_{1-x}Tb_xFe_2O_4$ ($0.0 \leq x \leq 0.2$) ferrites sintered at 1230 °C are shown in Figs. 1 and 2. The diffraction patterns were indexed on the basis of fcc lattice and the deduced parameters are listed in Table 1. The analysis of XRD patterns revealed that the samples with $0 \leq x \leq 0.04$ have single phase cubic spinel structure. A small peak of second phase appeared at $2\theta = 33.24^\circ$ for $x = 0.06$ and becomes more conspicuous for $x > 0.06$ as indicated in Figs. 1 and 2. This peak was identified as the (1 1 2) reflection of the $TbFeO_3$ (ortho ferrite) phase (ICDD PDF #47-0068). The second phase was not observed at $x = 0.08$ which might be overlapped in the background. The formation of second phase has also been reported when rare earth metal cations were substituted in Mn–Zn ferrites [10]. The following diffraction peaks of spinel structure corresponding to the planes (2 2 0), (3 1 1), (4 0 0), (4 2 2), (5 1 1/3 3 3) and (4 4 0) were observed. All the

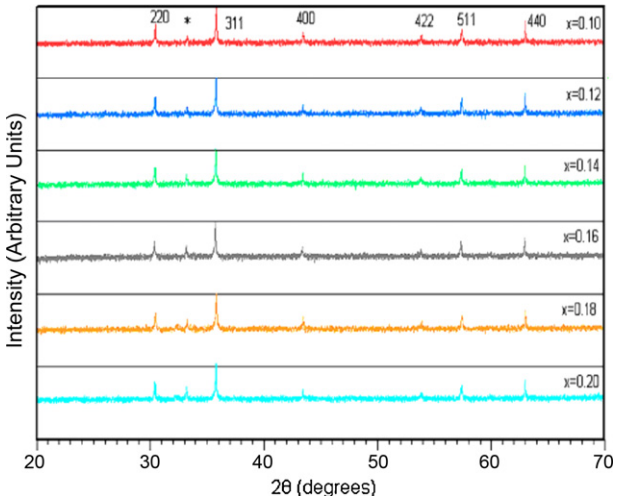

Fig. 2. X-ray diffraction patterns for $Mg_{1-x}Tb_xFe_2O_4$ ferrites ($x = 0.10$, 0.12, 0.14, 0.16, 0.18, 0.20).

Table 1
Phase, lattice constant, grain size, X-ray density and bulk density for $Mg_{1-x}Tb_xFe_2O_4$ ferrites ($0.0 \leq x \leq 0.2$).

Sr. No.	Composition	Secondary phase	Lattice constant (Å)	Grain size (μm)	X-ray density (D_x) (g/cm^3)	Bulk density (D_b) (g/cm^3)
1	$MgFe_2O_4$	–	8.361	3.46	4.55	3.5539
2	$Mg_{.98}Tb_{.02}Fe_2O_4$	–	8.3657	3.27	4.6	3.7155
3	$Mg_{.96}Tb_{.04}Fe_2O_4$	–	8.3669	3.18	4.66	3.8999
4	$Mg_{.94}Tb_{.06}Fe_2O_4$	$TbFeO_3$	8.3664	3.12	4.72	3.9296
5	$Mg_{.92}Tb_{.08}Fe_2O_4$	–	8.3662	3.05	4.78	4.1257
6	$Mg_{.9}Tb_{.1}$ Fe_2O_4	$TbFeO_3$	8.366	2.87	4.84	4.2909
7	$Mg_{.88}Tb_{.12}Fe_2O_4$	$TbFeO_3$	8.3653	2.79	4.91	4.3133
8	$Mg_{.86}Tb_{.14}Fe_2O_4$	$TbFeO_3$	8.3637	2.81	4.97	4.4676
9	$Mg_{.84}Tb_{.16}Fe_2O_4$	$TbFeO_3$	8.3641	2.62	5.03	4.4845
10	$Mg_{.82}Tb_{.18}Fe_2O_4$	$TbFeO_3$	8.3634	2.37	5.09	4.5605
11	$Mg_{.8}Tb_{.2}$ Fe_2O_4	$TbFeO_3$	8.3605	2.03	5.16	4.6063

mentioned peaks of the fcc lattice in the patterns matched well with the characteristic reflections of Mg-ferrite reported earlier [11]. The average grain size decreases with the increase of terbium concentration (Table 1) calculated by Scherrer's formula. The variation of lattice constants '*a*' with Tb-concentration (*x*) for $0.0 \leq x \leq 0.2$ is shown in Fig. 3. The lattice constant increases up to $x = 0.04$ and then decreases. The small increase in the lattice parameter with the increase of terbium contents (*x*) is attributed to the differences of the ionic radii of Tb^{3+} and Mg^{2+} ions. Since Tb^{3+} ion has larger ionic radius (0.93 Å) as compared to Mg^{2+} (0.66 Å), the partial replacement of Mg^{2+} by Tb^{3+} leads to the expansion of the spinel lattice; thereby increasing the lattice constant. It is therefore suggested that most of the replacement of Mg^{2+} ions by Tb^{3+} ions takes place on the octahedral sites as Tb ions are substituted for Mg ions. Gd-substituted ferrites also exhibited similar kind of results [12]. A slight decrease in the lattice constant '*a*' for $x > 0.04$ is due to the migration of few Mg^{2+} ions to tetrahedral sites owing to the incorporation of terbium ions on the octahedral sites. The decrease in '*a*' indicates the solubility limit for the terbium ions at $x = 0.04$. When the solubility limit is achieved no further terbium is dissolved in the spinel lattice and terbium ions accumulate to the grain boundaries combining with Fe to produce $TbFeO_3$ and form thin insulating layer around the grains. The appearance of secondary phase on the grain boundaries may suppress the grain growth by limiting the grain boundary mobility [13]. A non-

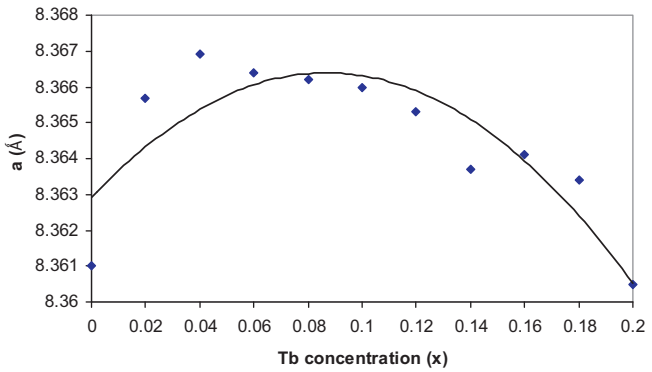

Fig. 3. Lattice parameter *a* vs Tb concentration for $Mg_{1-x}Tb_xFe_2O_4$ ferrites ($0 \leq x \leq 0.2$).

linear change of lattice constant '*a*' with concentration in spinel ferrites has also been reported earlier [14]. The Tb^{3+} ions may reside on B-sites as Tb^{3+} ions have larger ionic radius (0.93 Å) as compare to that of Fe^{3+} (0.64 Å) ions. The probability that terbium ions occupy the tetrahedral sites (A-sites) may be very remote. This is due to the fact that the tetrahedral sites are too small to be occupied by the large terbium ions. The internal stresses may also occur on B-sites where terbium ions occupy these sites due to their larger ionic radii. This result is in agreement with those already reported [15].

It is known that the site preference of Mg^{2+} ions in Mg-ferrite can be inferred from the intensities of the (2 2 0) and (4 4 0) planes [16]. A remarkable feature in the X-ray patterns of the present samples is the intensities of the (2 2 0) and (4 4 0) planes. The intensities of these two planes are found to increase with the increasing concentration of terbium compared to unsubstituted sample ($MgFe_2O_4$). This increase in intensity of (2 2 0) plane indicates that a fraction of Mg^{2+} ions migrate towards the A-sites when terbium is substituted in these ferrites. On the other hand increase in the intensity of (4 4 0) plane exhibits that the Mg^{2+} ions occupying on B-sites are substituted by the terbium ions. Hence Tb-substituted Mg-ferrites are predicted to be intermediate ferrites.

The bulk density of these ferrites increases with the increase of terbium concentration (*x*). The increase in bulk density is related to the higher atomic weights of Tb (158.92 amu) and its higher specific gravity (8.23 g/cm^3) compared to the atomic weights of Mg (24.3 amu) and the specific gravity of Mg (1.74 g/cm^3) atoms. The values of X-ray densities are larger in magnitude as compared to bulk densities and both the densities increase with the increase of terbium contents in these ferrites as listed in Table 1. The difference in the magnitude of these densities is owing to the existence of pores [17]. Both the densities increase linearly with the substitution of terbium contents. The substitution of terbium ions in magnesium ferrite causes an appreciable decrease in porosity ~21–10%. Hence densified samples have been obtained.

3.2. FTIR absorption studies

Fig. 4 shows representative room temperature FTIR spectra for Mg–Tb ferrites. FTIR spectra of the terbium (Tb)

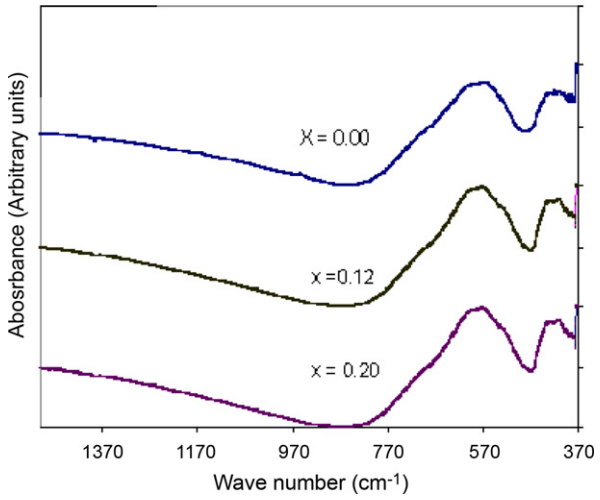

Fig. 4. FTIR spectra for $Mg_{1-x}Tb_xFe_2O_4$ ferrites ($x = 0.00$, 0.12, 0.20).

substituted Mg ferrites exhibit two absorption bands in the wave number range 370–1500 cm^{-1}. These bands are the characteristic features of the spinel ferrites [18]. The two absorption bands ν_1 and ν_2 are attributed to the intrinsic vibrations of the tetrahedral and octahedral group complexes, respectively. The tetrahedral (ν_1) and octahedral (ν_2) bands occur in the range 571–567 cm^{-1} and 429–418 cm^{-1}, respectively. The difference in the band position is caused by the difference in Fe^{3+}–O^{2-} distance for the octahedral and tetrahedral compounds. The band positions are tabulated in Table 2. The range of absorption bands obtained is in good agreement to the reported literature [19]. It is observed that ν_2 band is shifted towards lower frequencies with an increasing amount of terbium ions. The replacement of Mg^{2+} with Tb^{3+} ions (having larger ionic radius and higher atomic weight than Mg^{2+} and Fe^{3+}) on the octahedral sites in the ferrite lattice affects the Fe^{3+}–O^{2-} stretching vibrations. The octahedral band ν_2 seems to be continuously widened with Tb-concentration; this may be due to the statistical distribution of the Fe^{3+} ions on A- and B-sites [20]. The change in ν_1 band exhibits the drifting of Fe^{3+} ions towards oxygen ion on occupation of tetrahedral sites by few Mg^{2+} ions [16]. The change in the peak intensity of the spectra has been noticed with increasing Tb contents. It is well known that the intensity ratio is a function of the change of dipole moment with the inter-nuclear distance [21]. This ratio represents the contribution of the ionic bond Fe–O in the lattice. Hence the observed decrease in the peak intensity is attributed to the perturbation occurring in Fe–O bonds by the substitution of terbium ions.

Table 2
Fourier transform infrared spectroscopy (FTIR) absorption bands for $Mg_{1-x}Tb_xFe_2O_4$ ferrites ($x = 0$, 0.04, 0.08, 0.12, 0.16, 0.2).

Sr. No	Composition	ν_1 (cm^{-1})	ν_2 (cm^{-1})
1	$MgFe_2O_4$	571	429
2	$Mg_{0.96}Tb_{.04}Fe_2O_4$	567	428
3	$Mg_{0.92}Tb_{.08}Fe_2O_4$	571	427
4	$Mg_{0.88}Tb_{.12}Fe_2O_4$	566	425
5	$Mg_{0.84}Tb_{.16}Fe_2O_4$	566	419
6	$Mg_{0.8}Tb_{.2}Fe_2O_4$	567	418

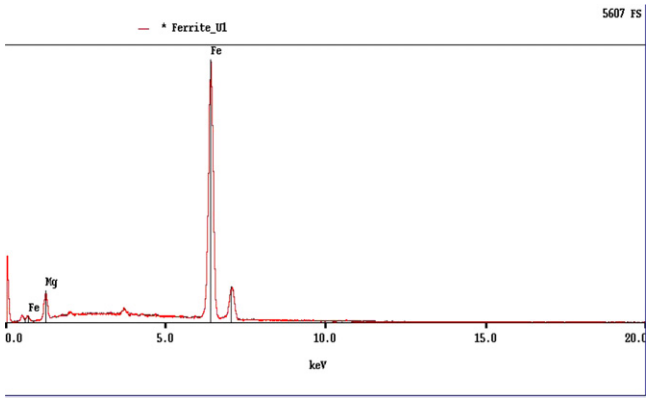

Fig. 5. EDX of the $MgFe_2O_4$ ferrite.

3.3. EDX analysis

Two representative EDX spectra are shown in Figs. 5 and 6. Fig. 5 represents pure Mg-ferrite while Fig. 6 indicates terbium substituted Mg-ferrite. EDX has been performed in order to study the compositional analysis. EDX analysis exhibits the elemental percentage of each element expected to be present in the ferrite sample. The heights of the peaks in the EDX graphs represent the proportion of each element in the finally sintered ferrite sample. A change has been observed in the size and height of the peaks of all the Tb-substituted samples. With the increase of Tb concentration, the graph exhibits an increase in the height of the Tb peaks. In the present study, the terbium is substituted for magnesium. Hence, the amount of magnesium decreases and this decrease in magnesium is observed in the peak height of Mg as shown in Fig. 6. The observed percentage of metals of each composition is consistent with the stoichiometry of the prepared samples.

3.4. Magnetic properties

The magnetic parameters saturation magnetization (M_s) and coercivity (H_c) are calculated from the MH loops (Figs. 7 and 8) of Mg–Tb ferrites and are plotted in Fig. 9. The saturation magnetization is increased at $x = 0.02$ and then decreases. The

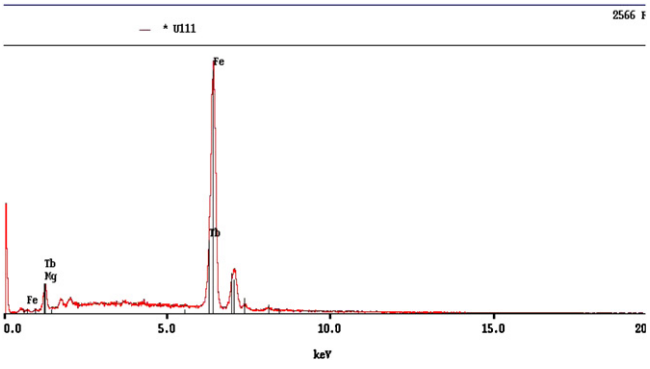

Fig. 6. EDX of the $Mg_{0.80}Tb_{0.20}Fe_2O_4$ ferrite.

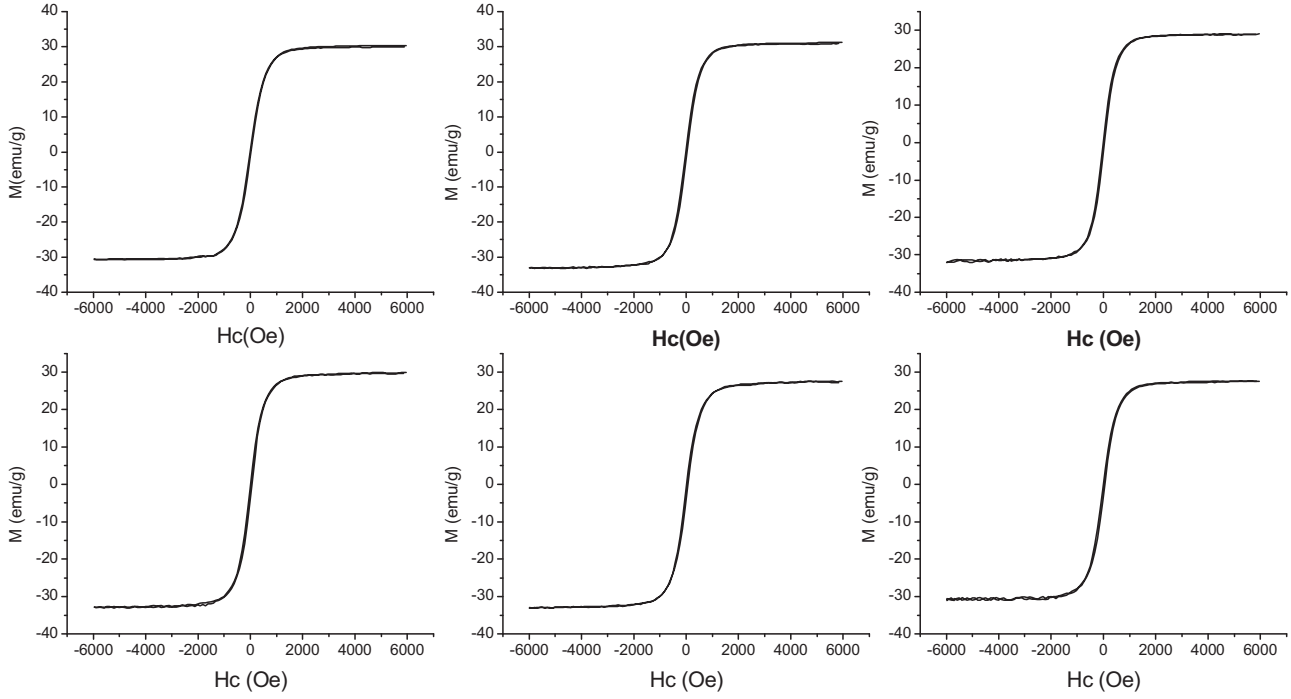

Fig. 7. MH loops of $Mg_{1-x}Tb_xFe_2O_4$ ferrites ($x = 0$, 0.02, 0.04, 0.06, 0.08, 0.1).

increase in saturation magnetization for $x = 0.02$ by the incorporation of terbium ions is attributed to the redistribution of cations on A- and B-sublattices. In $MgFe_2O_4$ ferrite most of the Mg^{2+} ions reside on B-sites and small fraction of these ions goes to the A-sites [22]. When terbium (Tb) ions are introduced into the octahedral sites few of the Mg^{2+} ions are migrated to the tetrahedral sites. These Mg^{2+} ions force equal amount Fe^{3+} ions to the octahedral sites [23], this increase the magnetization of the B-sublattice and hence the saturation magnetization of this composition increases.

The decrease in saturation magnetization for further substitution $x \geq 0.04$ of Tb^{3+} ions is owing to the magnetic disorder on B-sites caused by the presence of paramagnetic terbium ions on B-sites. It has been quoted that [24] the spin

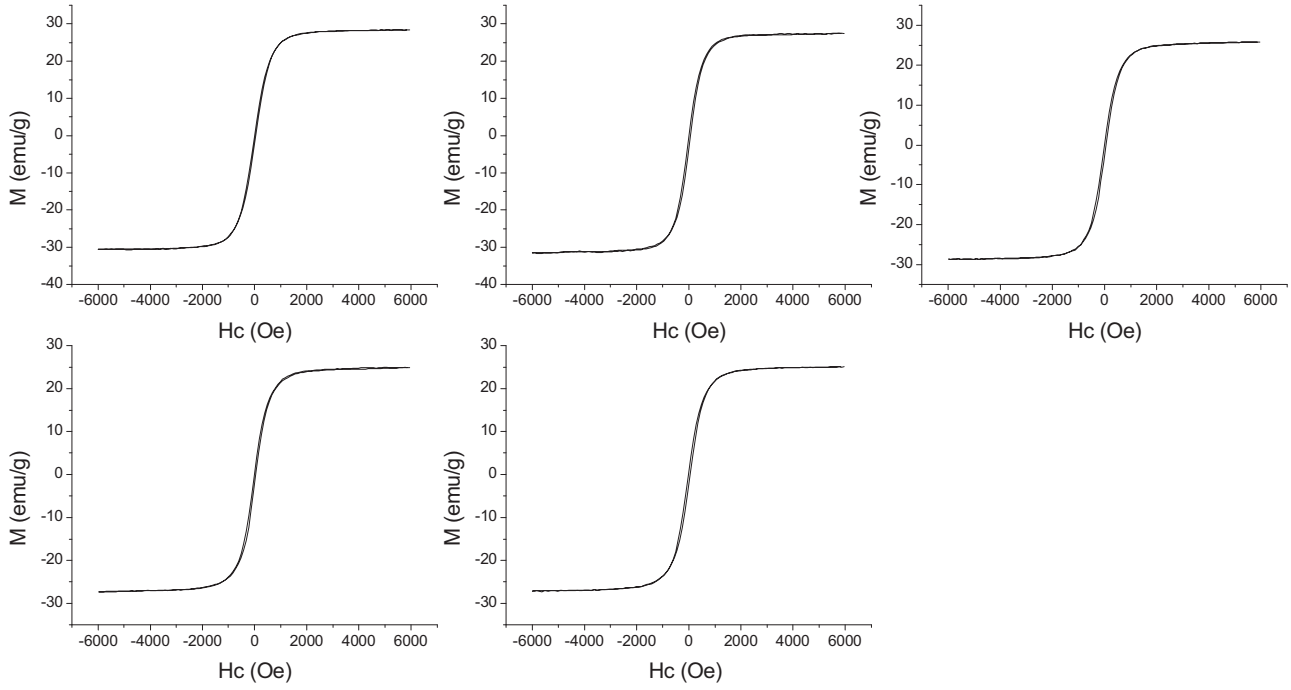

Fig. 8. MH loops of $Mg_{1-x}Tb_xFe_2O_4$ ferrites ($x = 0.12$, 0.14, 0.16, 0.18, 0.20).

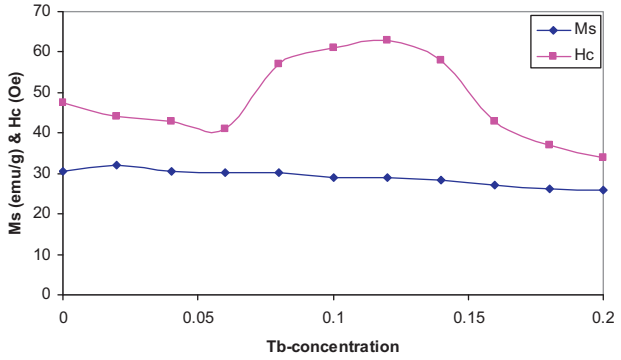

Fig. 9. Saturation magnetization (M_s) and coercivity (H_c) as a function of Tb content.

canting is caused by the substitution of rare earth ions, since Tb is a rare earth metal ion and it causes the transformation of collinear ferrimagnetic order into non-collinear arrangement of spins on B-sites. Hence the occupancy of Tb^{3+} ions on octahedral sites stemmed the collinear arrangement and reduces the saturation magnetization. Also no more Fe^{3+} ions are transferred to the octahedral sites which lead to the decrease of saturation magnetization. The decrease of saturation magnetization by the addition of rare earth ions in other ferrites has also been reported [25]. The site occupancy of Mg^{2+} and Fe^{3+} ions in Mg–Tb ferrites is complicated; however, the decrease of saturation magnetization for higher concentration of Tb^{3+} ions may be attributed to the secondary orthoferrite phase ($TbFeO_3$), which has a low value of magnetization. The decrease in the saturation magnetization with the evaluation of secondary phase has also been reported when Tb was substituted in Li–Zn ferrites [26].

The coercivity is found to decrease when Tb contents are increased up to $x = 0.06$ after which the coercivity increases. The coercivity has a linear relationship with porosity [27] for $0.00 \leq x \leq 0.06$ but for higher Tb concentration it deviates. The coercivity is the measure of magnetic field strength required for overcoming the magnetocrystalline anisotropy to flip the magnetic moments. For Tb-concentration $0.08 \leq x \leq 0.12$ the increase in coercivity is attributed to the dominant role of L–S coupling caused by the anisotropic terbium ions [28]. The increase in coercivity may also be related to the appearance of second phase on or near the grain boundaries which impede the motion of domain walls. The coercivity is decreased for higher concentration of Tb which could be due to the largest decrease in porosity.

3.5. Electrical properties

The dc electrical resistivity of $Mg_{1-x}Tb_xFe_2O_4$ ($0.00 \leq x \leq 0.2$) ferrites measured at room temperature with the increasing Tb concentration is shown in Fig. 10. The resistivity increases from 2.33×10^6 Ω-cm to 5.71×10^7 Ω-cm as the terbium concentration is increased from 0.02 to 0.2. The increase in resistivity of the Tb substituted samples is due to the larger resistivity value of Tb (111 μΩ-cm) as compared to Mg (4.3 μΩ-cm) atoms [29]. This increase may also be owing to the larger ionic radius of Tb^{3+} (0.93 Å) ions in comparison to Mg^{2+}

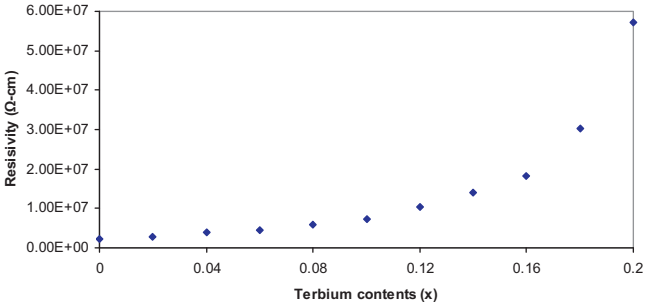

Fig. 10. Plot of room temperature resistivity (ρ) vs terbium concentration for $Mg_{1-x}Tb_xFe_2O_4$ ferrites.

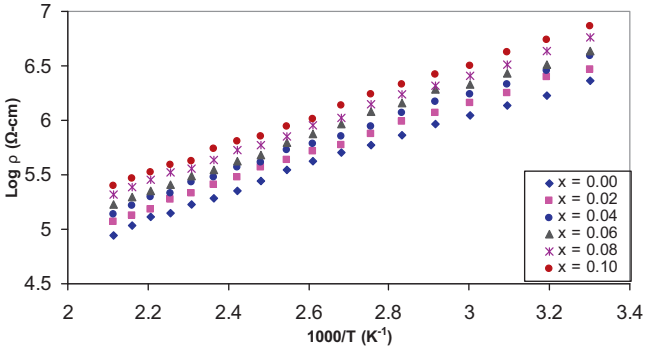

Fig. 11. Plot of log ρ vs $1000/T$ for $Mg_{1-x}Tb_xFe_2O_4$ ferrites ($0.00 \leq x \leq 0.10$).

(0.66 Å) ions which may increase the separation between the ferrous and ferric ions on the octahedral sites and impede the conduction phenomenon between these two ions [30].

Figs. 11 and 12 show temperature dependent electrical resistivity measured in the temperature range 30–200 °C. The temperature dependent resistivity indicates a linear relationship following well known Arrhenius relation [31]:

$$\rho = \rho_0 \exp\left(\frac{E_a}{k_B T}\right) \quad (4)$$

where ρ is the resistivity, ρ_0 is constant, E_a is the energy of activation and k_B is the Boltzmann's constant and T is the absolute temperature. The temperature dependent resistivity plots are used to calculate activation energy of hopping [32]. All these plots show that the resistivity decreases as the temperature increases, hence all the samples exhibit semi-

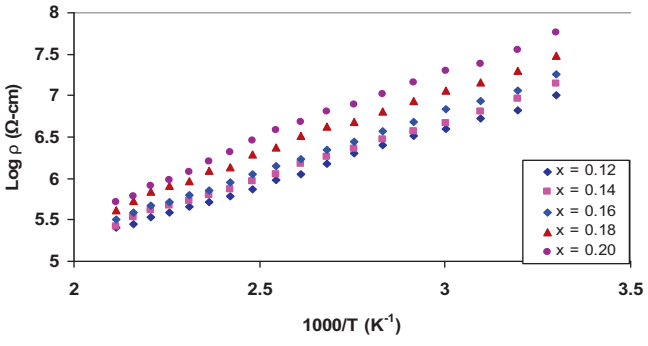

Fig. 12. Plot of log ρ vs $1000/T$ for $Mg_{1-x}Tb_xFe_2O_4$ ferrites ($0.12 \leq x \leq 0.20$).

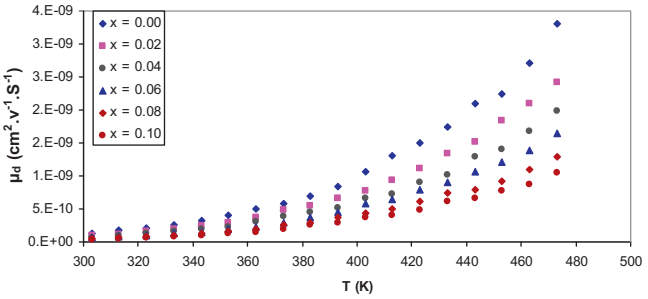

Fig. 13. The plot of drift mobility (μ_d) with temperature for $Mg_{1-x}Tb_xFe_2O_4$ ferrites ($0.00 \leq x \leq 0.10$).

conducting behaviour. Since all the samples show temperature dependence in the entire temperature range, therefore they may be called as degenerate type semiconductors. The drift mobility of all the compositions of $Mg_{1-x}Tb_xFe_2O_4$ ferrites have been calculated from the following relation [17]:

$$\mu_d = \frac{1}{ne\rho} \tag{5}$$

where 'e' is the charge on electron, ρ is the resistivity and 'n' is the concentration of charge carriers calculated from the following equation:

$$n = \frac{N_a \rho_a P}{M} \tag{6}$$

where N_a is the Avogadro's number, ρ_a is the bulk density of the sample, P is the number of iron atoms in the chemical formula of the sample and M is the molecular weight of the sample. The graphs of drift mobility vs temperature are shown in Figs. 13 and 14. The drift mobility increases with increasing temperature. The increase in drift mobility represents enhanced mobility of the charge carriers due to thermal activation. It may be due to the fact that as the temperature increases, the charge carriers start hopping from one site to another, hence the conduction process increases. Also Figs. 13 and 14 revealed that the samples having high resistivity have low value of drift mobility. The drift mobility drops from 1.26×10^{-10} to $4.49 \times 10^{-12}\,cm^2\,V^{-1}\,S^{-1}$ as the terbium concentration is increased from 0.00 to 0.2.

The Verwey's hopping model can be employed to explain the conduction mechanism in these ferrite systems. According to this model the conduction mechanism in ferrites is mainly attributed to the transfer of electrons between the ions of the same element occurring in more than one valence state, and these have random distribution on crystallographically equivalent lattice sites. The ferrites form closed packed oxygen lattices with the cations over the tetrahedral (A) and octahedral (B) sites. The separation between two metal ions residing on the octahedral (B) sites is smaller than the separation between a metal ion on the octahedral (B) sites and ion on the tetrahedral (A) sites. Hence the probability of electron hopping between octahedral (B) and tetrahedral (A) sites is very small as compared to the ions occurring on the octahedral (B) sites only. The electron hopping among the ions of the tetrahedral sites is not possible as there are only Fe^{3+} ions. The Fe^{2+} ions occupy only on octahedral sites. The hopping probability depends on the distance between the metal ions and the mobility of the charge carriers.

The presence of terbium ions on the octahedral sites (as discussed in FTIR analysis) increases the distance between the metal ions of the octahedral sites and impedes the electron transfer between the iron ions. The following conduction mechanism may also be possible in these ferrites:

$$Mg^{2+} + Fe^{3+} \leftrightarrow Mg^{3+} + Fe^{2+} \tag{7}$$

As Tb^{3+} ions are stable below 1300 °C and do not change their valence state from Tb^{3+} to Tb^{4+} ions. The incorporation of Tb^{3+} ions may cause in the blocking of the conduction mechanism. It is believed that Tb^{3+} ions behave like scattering centres in the electron exchange mechanism between the ions of different valencies situated on crystallographically equivalent positions in the lattice and enhances the resistivity of these ferrites.

The activation energy, deduced from the temperature variation of resistivity data as a function of terbium concentration is shown in Fig. 15. A small increase in the activation energy is observed up to $x = 0.10$ and later it increases more rapidly with increasing concentration of terbium ions. The higher activation energy values correspond to the higher resistivity values, due to the formation of insulating intergranular secondary phase ($TbFeO_3$) which impedes the conduction phenomenon. The increase in activation energy suggests the partial incorporation of terbium ions on the octahedral sites, which causes the blockage of electron transfer between the Fe^{3+} and Fe^{2+}. The activation energy values of the samples under investigation are comparable to the reported trivalent substituted magnesium ferrites [19].

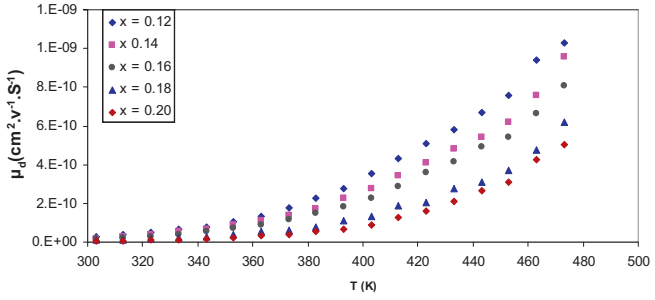

Fig. 14. The plot of drift mobility (μ_d) with temperature for $Mg_{1-x}Tb_xFe_2O_4$ ferrites ($0.12 \leq x \leq 0.20$).

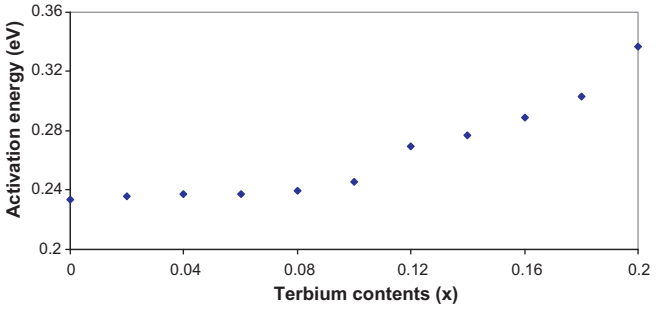

Fig. 15. Plot of activation energy vs terbium concentration for $Mg_{1-x}Tb_xFe_2O_4$ ferrites.

4. Conclusions

The present samples exhibit single phase spinel structure along with few traces of second phase $TbFeO_3$. The absorption bands observed in FTIR measurements ν_1 and ν_2 fall in the usual range of spinel ferrites. The decrease in the ν_2 band is related to the occupancy of Tb ions on the octahedral sites. The saturation magnetization is generally decreased by the terbium substitution due to spin canting on B-sites. The improvement in coercivity is attributed to the magneto-crystalline anisotropy of Tb ions. The dc electrical resistivity increases from 2.33×10^6 to 5.71×10^7 Ω-cm while the drift mobility drops with the increase of Tb contents up to $x = 0.2$.

Acknowledgements

The authors are highly thankful to Higher Education Commission of Pakistan for financial support for this work. We are grateful to Professor Carl E. Patton in the Department of Physics, Colorado State University, Fort Collins, USA for providing facilities for magnetic measurements.

References

[1] R. Tadi, K. Yong-Il, A.K. Sarella, C.G. Kim, K.-S. Ryu, Relation of structure and magnetic properties in nickel substituted $MgFe_2O_4$, J. Magn. Magn. Mater. 322 (2010) 3372–3376.
[2] E. Melagiriyappa, H.S. Jayanna, Structural and magnetic susceptibility studies of samarium substituted magnesium–zinc ferrites, J. Alloys Compd. 482 (2009) 147–150.
[3] M.A. Ahmed, E. Ateia, S.I. El-Dek, Rare earth doping effect on the structural and electrical properties of Mg–Ti ferrite, Mater. Lett. 57 (2003) 4256–4266.
[4] D.N. Bhosale, N.D. Choudhari, S.R. Sawant, P.P. Bakare, Initial permeability studies on high density Cu–Mg–Zn ferrites, J. Magn. Magn. Mater. 173 (1997) 51–58.
[5] P.P. Hankare, V.T. Vader, N.M. Patil, S.D. Jadhav, U.B. Sankpal, M.R. Kadam, B.K. Cougule, N.S. Gajbhiye, Synthesis, characterization and studies on magnetic and electrical properties of Mg ferrite with Cr substitution, Mater. Chem. Phys. 113 (2009) 233–238.
[6] Y.M.Z. Ahmed, E.M.M. Ewais, Z.I. Zaki, In situ synthesis of high density magnetic ferrite spinel ($MgFe_2O_4$) compacts using a mixture of conventional raw materials and waste iron oxide, J. Alloys Compd. 489 (2010) 269–274.
[7] J. Chand, M. Singh, Electric and dielectric properties of $MgGd_{0.1}Fe_{1.9}$ ferrite, J. Alloys Compd. 486 (2009) 376–379.
[8] B.D. Cullity, Elements of X-Ray Diffraction, Addison Wesley, USA, 1978
[9] M. Azhar Khan, M.U. Islam, M. Ishaque, I.Z. Rahman, A. Genson, S. Hampshire, Structural and physical properties of Ni–Tb–Fe–O system, Mater. Charact. 60 (2009) 73–78.
[10] M.A. Ahmed, N. Okasha, M.M. El-Sayed, Enhancement of the physical properties of rare earth substituted Mn–Zn ferrites prepared by flash method, Ceram. Int. 33 (2007) 49–58.
[11] M. Al-Haj, Structural characterization and magnetization of $Mg_{0.7}Zn_{0.3}Sm_xFe_{2-x}O_4$ ferrites, J. Magn. Magn. Mater. 299 (2006) 435–439.
[12] M.Z. Said, Effect of gadolinium substitutions on the structure and electrical conductivity of Ni-ferrite, Mater. Lett. 34 (1998) 305–307.
[13] N. Rezlescu, E. Rezlescu, P.D. Popa, L. Rezlescu, Effects of rare-earth oxides on physical properties of Li–Zn ferrite, J. Alloys Compd. 275–277 (1998) 657–659.
[14] N. Rezlescu, C. Doroftei, E. Rezlescu, P.D. Popa, Structure and humidity sensitive electrical properties of the Sn^{4+} and/or Mo^{6+} substituted Mg ferrite, Sens. Actuators B 115 (2006) 589–595.
[15] C.B. Kolekar, P.N. Kamble, A.S. Vaingankar, Structural and dc electrical resistivity study of Gd^{3+}-substituted Cu–Cd mixed ferrites, J. Magn. Magn. Mater. 138 (1994) 211–215.
[16] L. John Berchmans, R. Kalai Selvan, P.N. Selva Kumar, C.O. Augustin, Structural and electrical properties of $Ni_{1-x}Mg_xFe_2O_4$ synthesized by citrate gel process, J. Magn. Magn. Mater. 279 (2004) 103–110.
[17] M.U. Islam, M.A. Chaudhry, T. Abbas, M. Umar, Temperature dependent electrical resistivity of Co–Zn–Fe–O system, Mater. Chem. Phys. 48 (1997) 227–229.
[18] B.K. Labde, M.C. Sable, N.R. Shamkuwar, Structural and infra-red studies of $Ni_{1+x}Pb_xFe_{2-2x}O_4$ system, Mater. Lett. 57 (2003) 1651–1655.
[19] M.A. Ahmed, E. Ateia, F.M. Saleem, Spectroscopic and electrical properties of Mg–Ti ferrite doped with different rare-earth elements, Physica B 381 (2006) 144–155.
[20] S.C. Watawe, B.D. Sutar, B.D. Sarwade, B.K. Chougule, Infrared studies of some mixed Li–Co ferrites, Int. J. Inorg. Mater. 3 (2001) 819–823.
[21] S.A. Mazen, M.H. Abdallah, B.A. Sabrah, H.A.M. Hashem, The effect of titanium on some physical properties of $CuFe_2O_4$, Phys. Status. Solidi (a) 134 (1992) 263–271.
[22] N.N. Jani, B.S. Trivedi, H.H. Joshi, R.G. Kulkarni, Magnetic properties of the mixed spinel $Mg_{1+x}Mn_xFe_{2-2x}O_4$, Hyperfine Interact. 110 (1997) 227–237.
[23] M. Al-Haj, Structural and magnetic characterization of $Mg_xNi_{1-x}Sm_{0.02}$-$Sm_{0.02}Fe_{1.98}O_4$, Phys. Status Solidi (a) (2) 203 (2006) 343–348.
[24] Y. Wang, F. Xu, L. Li, H. Liu, H. Qiu, J. Jing, Magnetic properties of La-substituted Ni–Zn–Cr ferrites via rheological phase synthesis, Mater. Chem. Phys. 112 (2008) 769–773.
[25] L. Gama, A.P. Diniz, A.C.F.M. Costa, S.M. Rezende, A. Azevedo, D.R. Cornejo, Magnetic properties of nanocrystalline Ni–Zn ferrites doped with samarium, Physica B 384 (2006) 97–99.
[26] E. Rezlescu, N. Rezlescu, C. Pasnicu, M.L. Craus, P.D. Popa, Effects of rare-earth ions on the quality of a Li–Zn ferrite, Cryst. Res. Technol. 31 (1996) 343–352.
[27] A. Goldman, Modern Ferrite Technology, Van Nostrand Reinhold, New York, 1990.
[28] L. Ben Tahar, M. Artus, S. Ammar, L.S. Smiri, F. Herbst, M.-J. Vaulay, V. Richard, J.-M. Greneche, F. Villain, F. Fievet, Magnetic properties of $CoFe_{1.9}RE_{0.1}O_4$ nanoparticles (RE = La, Ce, Nd, Sm, Eu, Gd, Tb, Ho) prepared in polyol, J. Magn. Magn. Mater. 320 (2008) 3242–3250.
[29] C. Kittel, An Introduction to Solid State Physics, 5th ed., Wiley, New York/London, 1976.
[30] E. Rezlescu, N. Rezlescu, P.D. Popa, L. Rezlescu, C. Pasnicu, The influence of R_2O_3 (R = Yb, Er, Dy, Tb, Gd, Sm and Ce) on the electric and mechanical properties of a nickel–zinc ferrite, Phys. Status Solidi (a) 162 (1997) 673–678.
[31] M.U. Islam, F. Aen, B. Shahida, M. Niazi, M. Azhar Khan, M. Ishaque, T. Abbas, M.U. Rana, Electrical transport properties of CoZn ferrite–SiO_2 composites prepared by co-precipitation technique, Mater. Chem. Phys. 109 (2008) 482–487.
[32] M. Ishaque, M.U. Islam, M. Azhar Khan, I.Z. Rahman, A. Genson, S. Hampshire, Structural, electrical and dielectric properties of yttrium substituted nickel ferrites, Physica B 405 (2010) 1532–1540.